https://doi.org/10.5194/egusphere-2024-72
Preprint. Discussion started: 28 February 2024

Evaluation of CMIP6 Models Performance in Simulating Historical Biogeochemistry across Southern South China Sea

Winfred Marshal[1], Jing Xiang Chung [2], Mohd Fadzil Akhir [1]

[1]Institute of Oceanography and Environment, University Malaysia Terengganu, Kuala Nerus, Terengganu, Malaysia
[2]Faculty of Science and Marine Environment, Universiti Malaysia Terengganu, Kuala Terengganu 21030, Malaysia

Correspondence to: Jing Xiang Chung (jingxiang@umt.edu.my)

Abstract. This study evaluates the ability of Earth System Models (ESMs) from the Coupled Model Intercomparison Project Phase 6 (CMIP6) to simulate biogeochemical variables in the southern South China Sea (SCS). The analysis focuses on chlorophyll, phytoplankton, nitrate and oxygen at annual and seasonal scales. The models' performance is assessed against Copernicus Marine Environment Monitoring Service (CMEMS) data using statistical metrics such as the Taylor diagram and Taylor skill score. The results show that the models generally capture the observed spatial patterns of biogeochemical variables but exhibit varying degrees of overestimation or underestimation. The performance of the models is also influenced by the season, with some models showing better performance during the southwest monsoon than the northeast monsoon. Overall, the top five best-performing models for biogeochemical variables are MIROC-ES2H, GFDL-ESM4, CanESM5-CanOE, MPI-ESM1-2-LR and NorESM2-LM. The findings of this study have implications for researchers and end-users of the datasets, providing guidance for model improvement and understanding the impacts of climate change on the SCS ecosystem.

1 INTRODUCTION

Climate change has profound and wide-ranging effects on marine ecosystems, impacting both the physical environment and the primary productivity that inhabit it. Marine primary productivity plays a crucial role in sustaining life in the oceans and has far-reaching implications for the entire planet. Under climate change, understanding the importance of marine primary productivity becomes even more critical due to its various ecological, economic, and climate-related implications. For example, Henson et al. (2013) investigates the effect of climate change on the seasonal cycle of phytoplankton growth in the global ocean and finds that the seasonal amplitude of primary production is expected to decrease by 1–2% per year by 2100 in global ocean. These changes are driven by an increase in seasonal amplitude of sea surface temperature and suggested that the seasonality of primary production is more sensitive to climate change. Ocean Biogeochemistry (BGC) models are essential tools in understanding and simulating the interactions between the physical, chemical, and biological processes that occur in the ocean system. These models incorporate the cycling of key elements such as chlorophyll, phytoplankton, zooplankton, carbon, nitrogen, phosphorus, oxygen, etc., through the atmosphere and ocean ecosystems. The importance of

https://doi.org/10.5194/egusphere-2024-72
Preprint. Discussion started: 28 February 2024

ocean BGC models lies in their ability to provide a more comprehensive and integrated understanding of the marine environment. The reliability and accuracy of climate projections made by climate models are closely tied to how well these models are able to replicate or simulate past climate conditions (Jia et al., 2023; Shikha and Valsala, 2018; Tang et al., 2021). If a model successfully reproduces historical climate patterns, it indicates that the model has captured and represents the relevant physical processes and interactions within the Earth's system. This gives the confidence that the model is a reliable tool for making future climate projections. As part of the World Climate Research Programme (WCRP), the Coupled Model Intercomparison Project Phase 6 (CMIP6) oversees the implementation of General Circulation Models (GCMs) by multiple modeling institutions, aiming to simulate the Earth's climate system behaviour to study a wide range of climate-related phenomena such as climate variabilities and past & future climate projection (Mohanty et al., 2024; Peng et al., 2021; Pereira et al., 2023; Petrik et al., 2022). This simulation aims to explore how Earth's climate responds to various climate forcing under distinct scenarios known as "Socioeconomic pathways (SSPs)". The intention is to provide a broader array of potential futures for simulation studies (Riahi et al., 2017). For example, Kwiatkowski et al. (2020) indicates that forthcoming climate change is anticipated to exert a noteworthy and adverse influence on ocean biogeochemistry across different CMIP6 Shared Socioeconomic Pathways (SSPs). Specifically, the low-emission scenario SSP1-2.6 and the high-emission scenario SSP5-8.5 are projected to induce moderate to highly severe alterations. By the conclusion of the 21st century, global mean sea surface temperature is expected to rise, while surface pH, subsurface oxygen and nitrate concentration are anticipated to decrease. These transformations are likely to negatively affect ocean productivity, resulting in a global mean decline. The performance of CMIP6 models varies more at the regional scale than at the global scale (Oh et al., 2023). This is because regional climate features are more sensitive to the details of the models' representations of physical processes, such as cloud formation, convection, submesoscale eddies, wave-interactions, etc. However, before we can leverage GCMs to study regional biogeochemical changes, rigorous performance testing is needed. These tests ensure the accuracy and reliability of model results, paving the way for reliable future studies.

There are few studies have evaluated the effectiveness of CMIP6 ocean models in simulating different biogeochemical variables over the globe scale but Intercomparison of CMIP6 BGC model’s performance and ranking them according to their performance skill in regional scale had not done yet. For example, Petrik et al. (2022) evaluates the representation of mesozooplankton in six CMIP6 Earth System Models (ESMs) and compared the models' simulated mesozooplankton biomass and distribution to observations and assess their ability to capture the observed relationship between mesozooplankton and chlorophyll-a and finds that the six CMIP6 ESMs generally represent the large regional variations in mesozooplankton biomass at the global scale. Three of the ESMs simulate a mesozooplankton-chlorophyll relationship within the observational bounds, which can be used as an emergent constraint on future mesozooplankton projections. However, there is a wide ensemble spread in projected changes in mesozooplankton biomass, reflecting the uncertainties in the models' representation of mesozooplankton in global scale. Tjiputra et a. (2020) provides an in-depth assessment of the ocean biogeochemistry component of the Norwegian Earth System Model (NorESM2) and discussed the implications of their findings for understanding and predicting future ocean biogeochemical changes in global scale.

https://doi.org/10.5194/egusphere-2024-72
Preprint. Discussion started: 28 February 2024

NorESM2 represents a significant advancement in ocean BGC modeling, incorporating a comprehensive representation of biogeochemical processes and demonstrating improved skill in simulating observed ocean biogeochemical properties. Similarly, Christian et al. (2022) presents a comprehensive overview of the ocean BGC components of two new versions of the Canadian Earth System Model (CanESM), CanESM5 and CanESM5-CanOE and describe the models in detail and compare their performance against observations and other CMIP6 models in global scale. CanESM5-CanOE shows improved skill relative to CanESM5 for most major tracers at most depths. However, both CanESM5 models have some biases, such as an underestimation of surface nitrate concentrations in the subarctic Pacific and equatorial Pacific and an overestimation in the Southern Ocean. This opens a way to perform more regional Intercomparison skill assessments on CMIP6 BGC models.

Sunda shelf region of southern South China Sea (SCS) is located in the center of the Southeast Asian monsoonal system with heavy precipitation rates (You and Ting, 2021), river input that deliver freshwater (Lee et al., 2019), dissolved nutrients (Jiang et al., 2019) and surrounded by volcanic islands, the Himalaya in the background, this region is characterized by one of the largest sediment discharge rates worldwide (Milliman et al., 1999). The Sunda Shelf Sea in Southeast Asia stands out as one of the world's largest and most diverse shelf seas. Despite its ecological significance, it faces considerable human population density along its coastline, leading to substantial stress on its marine habitats. This is particularly evident in urbanized marine ecosystems exposed to significant human-induced pressures (Todd et al., 2019). Concurrently, our knowledge of the biogeochemistry of tropical shelf seas lags behind that of higher-latitude environments, posing challenges in predicting the impact of anthropogenic pressures on tropical seas (Lønborg et al., 2021). This calls for the need for credible future BGC projections to help devise appropriate mitigation measures to curb and mitigate the impacts of climate change in this region. Based on this backdrop, this study objectively aims at ranking 13 CMIP6 ocean models' historical simulations based on their ability to reproduce the selective observed biogeochemical variables such as chlorophyll, phytoplankton, nitrate and oxygen over the southern SCS. The rest of this paper will be structured as follows: Section 2 gives a brief description of the study domain and the dataset used. Section 3 will elaborate the methodology employed. Section 4 presents the results and discussion under sub-topics; spatial variation and bias, Taylor diagram and model ranking. Conclusion of the study is summarized in Section 5.

2 STUDY DOMAIN AND DATA

2.1 Study domain

This study focuses on the Sunda shelf region, also referred to as the southern SCS, delineated by latitudes 8°S – 15°N and longitudes 98°E – 121°E, as illustrated in **Fig. 1**. Situated within the tropical rim of the Northwestern Pacific Ocean, this region is an integral part of one of the world's largest marginal seas, the SCS. The southern SCS is characterized by a shallow bathymetry, with a maximum depth of approximately 100 meters, except for the central part, where depths exceed

https://doi.org/10.5194/egusphere-2024-72
Preprint. Discussion started: 28 February 2024

1,000 meters. The region's circulation and hydrodynamics are strongly influenced by monsoonal winds, along with other factors such as complex bathymetry, coastline configuration, the presence of large islands, river discharge, mixing, upwelling, internal waves, and eddies (Daryabor et al., 2014, 2015).

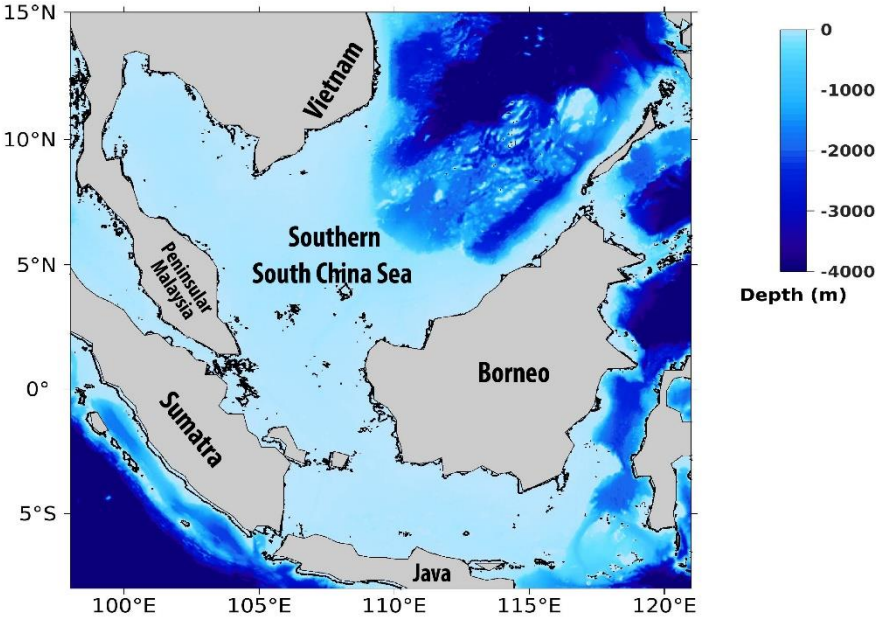

Figure 1. Map and bathymetry of the study domain

2.2 Datasets

Within the southern SCS, extensive observations have demonstrated that phytoplankton growth, the primary source of organic matter, plays a crucial role in regulating oceanic carbon cycles and exhibits a sensitive response to monsoon-driven physical-biogeochemical processes. These processes enhance mixing throughout the basin, influencing the overall nutrient supply and primary productivity in the euphotic zone (Palacz et al., 2011; Tseng et al., 2005). Therefore, chlorophyll, phytoplankton, nitrate and oxygen are the primary biogeochemical variables examined in this study. We analysed the historical experiment outputs of 13 CMIP6 ESMs for the study region. The model designations and spatial resolutions are provided in **Table 1**. This selection was based on the common availability of the chosen variables and their corresponding socioeconomic scenario projections at the time of this study. The selection of the evaluation period was primarily based on the availability of reference datasets for comparison with the model outputs. The Copernicus Marine Environment Monitoring Service (CMEMS) data (von Schuckmann et al., 2020), a standardized collocated grid with a horizontal resolution of 1/4 degree (approximately 27 km) and temporal coverage from 1993 onwards, was chosen as the reference dataset to assess the models' ability to simulate biogeochemical variables over the southern SCS. By methodically

https://doi.org/10.5194/egusphere-2024-72
Preprint. Discussion started: 28 February 2024

115 contrasting the biogeochemical simulated fields with a variety of gridded datasets, such as Ocean Colour and World Ocean Atlas 2013, the quality of this data was evaluated. Mercator-Ocean has previously recorded this evaluation in the Quality Information Document (QuID) (Perruche et al., 2019). Furthermore, the evaluation method relies on the analysis of an average year to represent the regional climatology. A longer period is generally considered more representative, and within the constraints of data availability, the 22-year period from 1993 to 2014, encompassing the end of the CMIP6 historical
120 experiments, was selected. As the CMIP6 models have different horizontal scales, all model outputs were regridded to a common horizontal resolution using the bilinear interpolation method. The CMIP6 climate models are publicly available and archived at https://esgf-node.llnl.gov/search/cmip6/, while the CMEMS data can be accessed at https://data.marine.copernicus.eu/products.

125 **Table 1.** List of 13 CMIP6 models used including model name, modeling institution, coupled BGC Model and the horizontal resolution.

Model Abbreviation	Institution	BGC Model	Horizontal Resolution	References
ACCESS-ESM1-5	CSIRO, Australia	WOMBAT	250 km	(Ziehn et al., 2020)
CanESM5	CCCma, Canada	CMOC	100 km	(Swart et al., 2019)
CanESM5-CanOE		CanOE		
GFDL-ESM4	NOAA-GFDL, USA	COBALTv2	1° x 1° degree	(Dunne et al., 2020)
MIROC-ES2H	MIROC, Japan	OECO2	100 km	(Kawamiya et al., 2020)
MIROC-ES2L				(Hajima et al., 2020)
MPI-ESM-1-2-HAM	Consortium of Switzerland, Germany, UK, Finland	HAMOCC6	220 km	(Neubauer et al., 2019)
MPI-ESM1-2-HR	Max Planck Institute for Meteorology, Germany		50 km	(Müller et al., 2018)
MPI-ESM1-2-LR			220 km	(Mauritsen et al., 2019)
MRI-ESM2-0	Meteorological Research Institute, Japan	MRI.COM4.4	100 km	(Yukimoto et al., 2019)
NorESM2-LM	NCC, Norway	iHAMMOC	100 km	(Tjiputra et al., 2020)
NorESM2-MM				
UKESM1-0-LL	Met Office Hadley Centre, UK	MEDUSA2	100 km	(Sellar et al., 2019)

https://doi.org/10.5194/egusphere-2024-72
Preprint. Discussion started: 28 February 2024

3 METHODOLOGY

3.1 Evaluation metrics and Ranking

To evaluate the ability of CMIP6 models to simulate biogeochemical variables in comparison to CMEMS data, spatial variation, Mean Bias Error (MBE), Correlation Coefficient (CC), Root Mean Square Difference (RMSD), and Normalized Standard Deviation (NSD) were employed. CC, RMSD, and NSD were calculated using Taylor Diagram (TD) which offers a succinct statistical summary of the degree of similarity in patterns between simulated and observed data based on their CC, RMSD, and variance ratio. Smaller values of RMSE and BIAS indicate better model performance, while a larger positive value of CC, ranging from -1 to 1, suggests improved correlation between the simulated and observed climate variables. The specific equations used to calculate MBE and CC, RMSD and SD using TD are presented in equations (1) – (4), respectively.

$$\mathrm{MBE} = \frac{1}{n}\sum_{i=1}^{n}(M_i - R_i) \quad (1)$$

$$\mathrm{CC} = \frac{\sum_{i=1}^{n}(M_i - \bar{M})\,(R_i - \bar{R})}{\sqrt{\sum_{i=1}^{n}(M_i - \bar{M})}\sqrt{\sum_{i=1}^{n}(R_i - \bar{R})}} \quad (2)$$

$$\mathrm{RMSD} = \sqrt{\frac{1}{n}\sum_{i=1}^{n}(M_i - R_i)^2} \quad (3)$$

$$SD = \sqrt{\frac{1}{n}\sum_{i=1}^{n}(M_i - \bar{M})^2} \quad (4)$$

$$TSS = \frac{(1+R)^4}{4\left(SDR + \frac{1}{SDR}\right)^2} \quad (5)$$

Where ‘n’ represents the total number of grids within the ocean areas of the analysis domain, and M_i and $\bar{R}$ denote the model and reference at i^{th} grid, respectively. $\bar{M}$ and $\bar{R}$ represent the mean values of the model and the reference data.

The assessment of model performance hinges on various factors, including the specific variables, the regions under analysis, and the chosen evaluation metrics. Achieving a fair and standardized comparison necessitates consideration of these elements. In this context, models were ranked based on their performance utilizing the Taylor Skill Score (TSS), as outlined in equations (5). Here, 'R' signifies the pattern correlation between the models and the reference data, while 'SDR'

https://doi.org/10.5194/egusphere-2024-72
Preprint. Discussion started: 28 February 2024

stands for the ratio of the spatial standard deviations of the models to that of the reference. The Taylor Skill Score quantifies the resemblance between the model and reference data concerning both the distribution and amplitude of the spatial pattern (Taylor, 2001). All evaluation metrics were applied to each variable, leading to the generation of individual and overall rankings for the models. All analyses in this study were conducted using MATLAB software and its numerical functionalities; Scientific colour maps 7.0 was used to make figures that are readable by readers with colour vision impairments (Crameri et al., 2020, 2021).

4 RESULTS & DISCUSSION

4.1 Spatial variation & Bias

Although temporal cycles, such as the yearly cycle of seasons, play a crucial role in climate variability, they do not fully capture the long-term changes associated with climate change. In contrast, spatial patterns provide a more comprehensive understanding of how climate is changing across different regions and ecosystems (Chi et al., 2023). Consequently, the spatial distributions of each biogeochemical variable were analysed seasonally, during the southwest and northeast monsoons, and compared to reference data. This approach provides a general overview of the models, their differences from observations, and their relative performance. The months June, July, and August (JJA) as southwest (summer) and December, January, and February (DJF) as northeast (winter) were selected to represent the respective seasons. Seasonal variations and their mean bias are presented in **Fig. 2 - 5**, demonstrating the ability of each model to reproduce the seasonal distribution for the southern SCS region. While most CMIP6 climate models effectively capture the observed seasonal pattern of each biogeochemical variable, some models exhibit overestimations or underestimations of the observed magnitude.

Three ESMs, namely ACCESS-ESM1-5, CanESM5-CanOE, and MPI-ESM1-2-HR, consistently showed an overestimation of chlorophyll concentrations during both the DJF and JJA seasons **(Fig. 2a, b)**. Their mean biases surpassed 0.3 mg/m^3, indicating a notable discrepancy between the simulated and observed chlorophyll levels **(Fig. 2c)**. This overestimation raises concerns about potential shortcomings in these models' representation of biogeochemical processes governing phytoplankton growth and chlorophyll production. In contrast to the overestimating models, CanESM5 consistently underestimated chlorophyll concentrations in both seasons, with a mean bias of -0.02 mg/m^3. This suggests that the model consistently generated chlorophyll values lower than those observed. Possible explanations for this underestimation could be an underrepresentation of nutrient availability or an overestimation of grazing pressure on phytoplankton. The remaining ESMs, including the model ensemble, demonstrated a moderate ability to replicate observed chlorophyll concentrations. Their mean biases generally fell within an acceptable range, indicating that these models capture the overall patterns of chlorophyll distribution in the South China Sea. Three models, namely CanESM5-CanOE, MPI-ESM1-2-HR, and UKESM1-0-LL, consistently overestimated phytoplankton carbon levels in both seasons **(Fig. 3a, b)**,

https://doi.org/10.5194/egusphere-2024-72
Preprint. Discussion started: 28 February 2024

exhibiting mean biases exceeding 1 mmol/m^3. This overestimation suggests potential shortcomings in these models' representation of phytoplankton growth and carbon fixation processes. In contrast, CanESM5 exhibited a persistent underestimation of phytoplankton carbon throughout the year. Its mean bias of -0.9 mmol/m^3 **(Fig. 3c)** highlights a discrepancy between simulated and observed phytoplankton carbon levels. This underestimation could stem from factors such as an overestimation of zooplankton grazing or an underestimation of phytoplankton productivity. The remaining ESMs, with the exception of CanESM5, moderately replicated the observed phytoplankton carbon patterns. Their mean biases were generally within an acceptable range.

https://doi.org/10.5194/egusphere-2024-72
Preprint. Discussion started: 28 February 2024

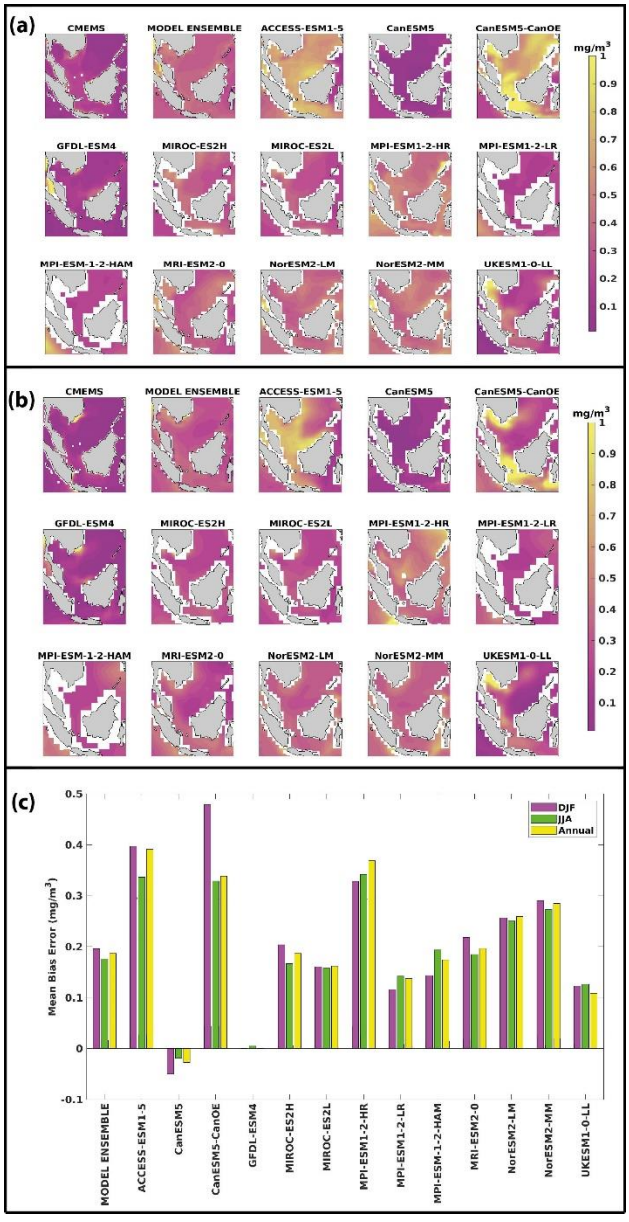

Figure 2. The seasonal climatology of surface chlorophyll for CMEMS, model ensemble and 13 individual models during (a) DJF and (b) JJA. Additionally, bar graph (c) illustrates the mean bias errors in their seasonal and annual mean.

https://doi.org/10.5194/egusphere-2024-72
Preprint. Discussion started: 28 February 2024

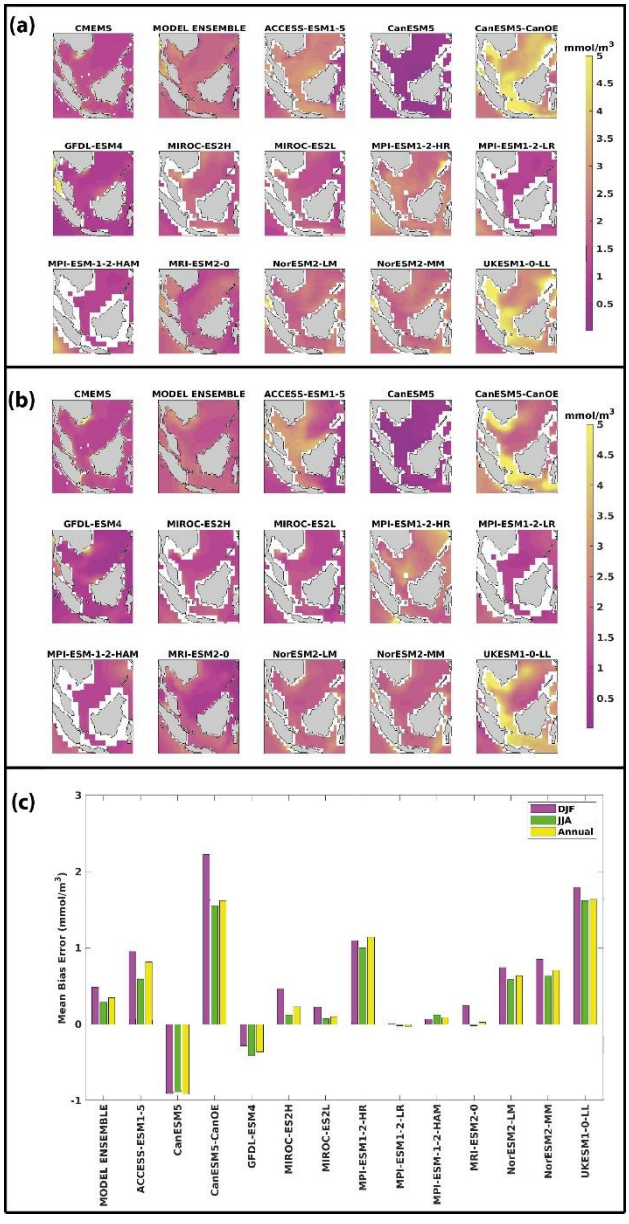

Figure 3. The seasonal climatology of surface phytoplankton for CMEMS, model ensemble, and 13 individual models during (a) DJF and (b) JJA. Additionally, bar graph (c) illustrates the mean bias errors in their seasonal and annual mean.

205 The analysis revealed a divergent pattern among ESMs in replicating observed nitrate concentrations in both seasons **(Fig. 4a, b)**. ACCESS-ESM1-5 exhibited an extreme overestimation of nitrate levels, with a mean bias of 2.1 mmol/m^3, suggesting potential shortcomings in the model's representation of nitrate uptake by phytoplankton or denitrification processes. GFDL-ESM4, NorESM2-LM, and NorESM-2MM also displayed substantial overestimations, with

https://doi.org/10.5194/egusphere-2024-72
Preprint. Discussion started: 28 February 2024

mean biases exceeding 0.5 mmol/m^3 **(Fig. 4c)**. These overestimations could stem from factors such as an underestimation of nitrate removal processes or an overestimation of nutrient inputs from rivers. The remaining ESMs moderately replicated the observed nitrate patterns, indicating a reasonable representation of nitrate dynamics in these models. Three models, namely MIROC-ES2H, MPI-ESM1-2-LR, and MPI-ESM-1-2-HAM, consistently overestimated oxygen levels in both seasons **(Fig. 5a, b)**, exhibiting mean biases exceeding 2 mmol/m^3. This overestimation suggests potential shortcomings in these models' representation of oxygen production through photosynthesis or oxygen consumption through respiration and microbial processes. Conversely, ACCESS-ESM1-5 and CanESM5 displayed persistent underestimations of oxygen throughout the year. Their mean biases exceeding -2 mmol/m^3 highlight a discrepancy between simulated and observed oxygen levels **(Fig. 5c)**. This underestimation could stem from factors such as an overestimation of oxygen consumption processes or an underestimation of oxygen production through photosynthesis. The remaining ESMs moderately replicated the observed oxygen patterns. Their mean biases were generally within an acceptable range.

https://doi.org/10.5194/egusphere-2024-72
Preprint. Discussion started: 28 February 2024

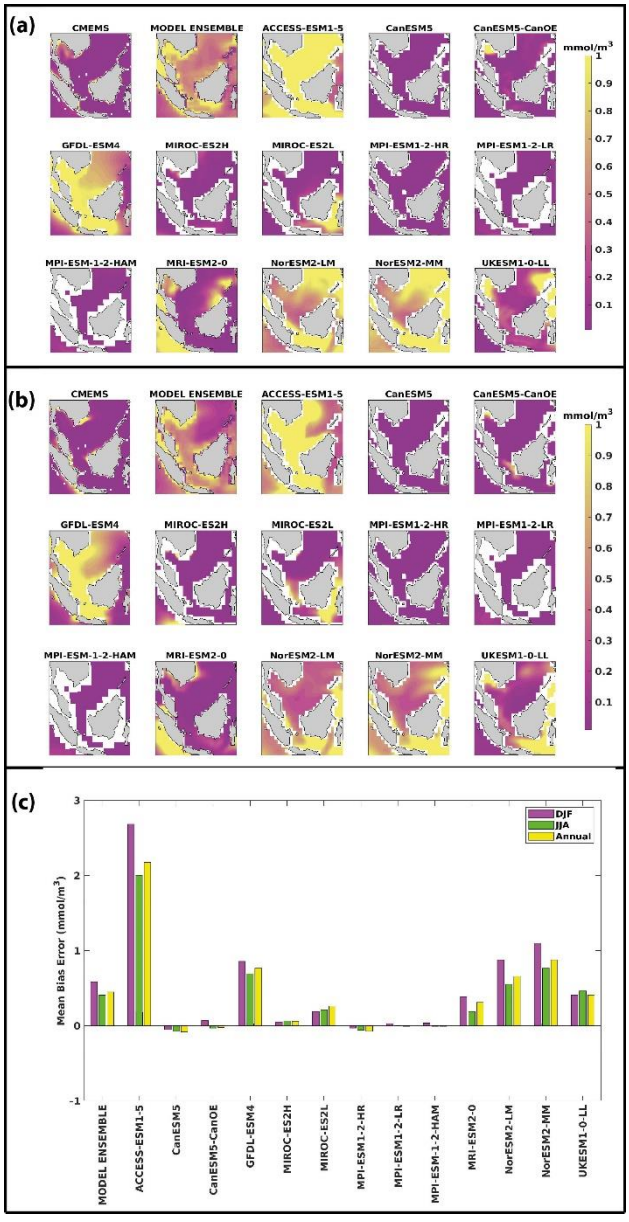

Figure 4. The seasonal climatology of surface nitrate for CMEMS, model ensemble, and 13 individual models during (a) DJF and (b) JJA. Additionally, bar graph (c) illustrates the mean bias errors in their seasonal and annual mean.

https://doi.org/10.5194/egusphere-2024-72
Preprint. Discussion started: 28 February 2024

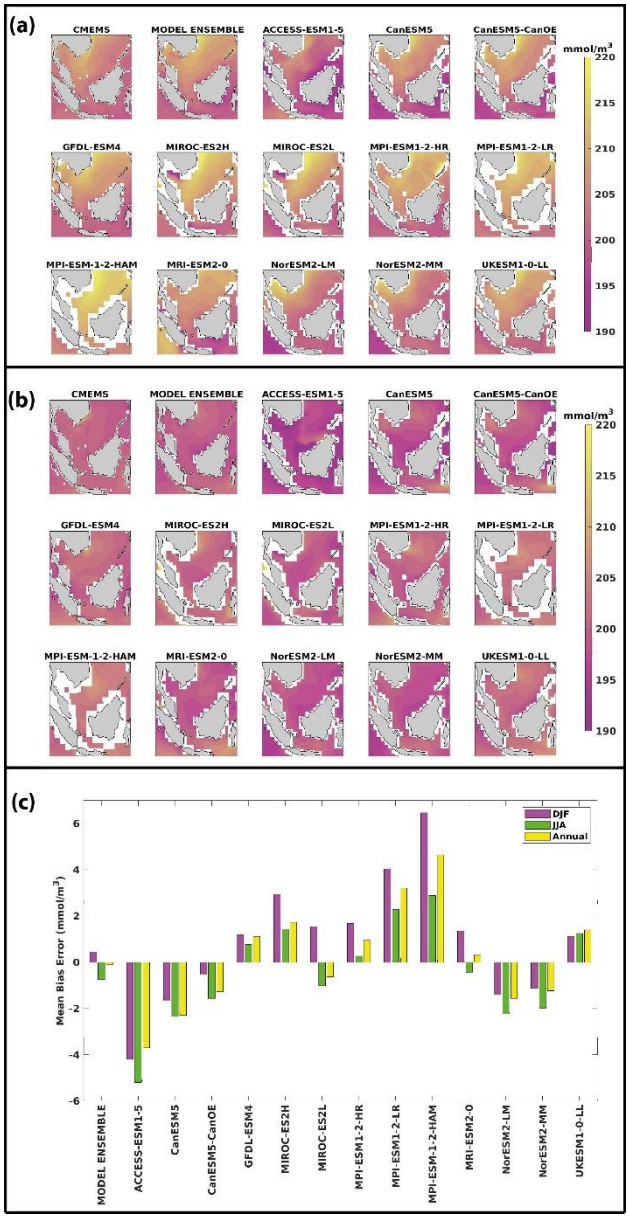

Figure 5. The seasonal climatology of surface oxygen for CMEMS, model ensemble, and 13 individual models during (a) DJF and (b) JJA. Additionally, bar graph (c) illustrates the mean bias errors in their seasonal and annual mean.

The observed bias underscores the necessity of error correction, as these errors are likely to persist in the projections (SSPs), potentially introducing significant uncertainty. The flow of nutrients and other biogeochemical tracers around the globe is significantly influenced by ocean circulation patterns. Alterations in these patterns can lead to shifts in nutrient distribution, consequently impacting biogeochemical processes (Lu et al., 2020). In southern SCS, ocean circulation exhibits

https://doi.org/10.5194/egusphere-2024-72
Preprint. Discussion started: 28 February 2024

substantial variations driven by the monsoon cycle (Gan et al., 2016). During the northeast monsoon, spanning December to February, winds prevail from the northeast, generating a basin-wide cyclonic gyre within the southern SCS. Conversely, during the southwest monsoon, from June to August, winds blow from the southwest, establishing a double-gyre circulation pattern in the southern SCS. The transition between the northeast monsoon and southwest monsoon circulation patterns is gradual, occurring over several weeks. While the timing of this transition varies from year to year, it typically takes place in April and October. The monsoon-driven circulation in the southern SCS has significant implications for the region's biogeochemistry and marine ecosystems. For instance, the northward currents during the southwest monsoon transport nutrients from the equator to the northern SCS, fostering high levels of productivity in this region. Conversely, the southward currents during the northeast monsoon transport nutrients from the northern SCS to the equator, where they are utilized by phytoplankton and other marine organisms (Liu et al., 2002).

It is important to note that not all CMIP6 ESMs fail to reproduce the observed seasonal pattern of biogeochemistry, and it is unrealistic to expect a single ESM to accurately represent all biogeochemical variables. While some ESMs can effectively reproduce the observed pattern for individual variables, there remains significant uncertainty regarding the reasons why some ESMs outperform others in this respect. The ESMs employed in CMIP6 are influenced by a variety of external factors, including solar radiation, greenhouse gas concentrations, and land-use changes. These external forcing are typically incorporated into ESMs as time-series data. Inaccuracies in these time-series data can lead to discrepancies in the simulated biogeochemistry, including errors in the seasonal cycle (Sun and Mu, 2021). Even the most advanced ESMs do not fully capture all of the biogeochemical processes that occur in the real world. This implies that some ESMs may overlook important processes that contribute to the observed seasonal pattern of biogeochemistry. Additionally, the ability of an ESM to replicate the observed seasonal pattern of biogeochemistry can be influenced by the model's resolution and the specific numerical methods used to solve its equations.

4.2 Taylor's diagram

The Taylor diagram was used to evaluate and summarize the performance of CMIP6 models across various parameters they simulated. Taylor diagram provide a concise and visually appealing way to compare the performance of multiple models against observational data. Taylor diagrams facilitate the inter-comparison of multiple CMIP6 ESMs, allowing researchers to identify models that consistently perform well or poorly across a range of biogeochemical parameters by incorporate three key metrics: correlation coefficient, normalized standard deviation and normalized root mean squared difference. These metrics collectively evaluate the agreement between model simulations and observations in terms of their overall pattern, magnitude, and phase relationship by baseline observed point where the correlation is 1 and the RMSD is 0. If the simulation point is close to the observed point, it means that both the model and reference data are highly similar. Taylor diagrams can be applied to assess model performance at regional and seasonal scales, providing insights into the models' ability to capture spatial and temporal variations in biogeochemical processes. This information can be valuable for understanding regional

https://doi.org/10.5194/egusphere-2024-72
Preprint. Discussion started: 28 February 2024

climate-biogeochemistry interactions. Taylor diagram for assessing the selected models were performed based on their annual climatology.

Regarding chlorophyll, overall performance of the 13 CMIP6 ESMs in simulating chlorophyll spatial patterns was moderate, with spatial correlations ranging from -0.2 to 0.7 and RMSDs below 2 **(Fig. 6a)**. MIROC-ES2H and MIROC-ES2L were the best performing models, with correlation coefficients of 0.6 and 0.4, RMSDs of 0.7 and 0.9, and standard deviations of 0.6 and 0.5, respectively when compared to other models. ACCESS-ESM1-5 and UKESM1-0-LL had the poorest performance, with correlation coefficients of 0.1 and 0.2, RMSDs of 2.1 and 1.8, and standard deviations of 2 and 1.7, respectively. Similar to chlorophyll, the performance of the ESMs in simulating phytoplankton spatial patterns was moderate **(Fig. 6b)**. MIROC-ES2H was the best performing model, with a correlation coefficient of 0.4, an RMSD of 0.9, and a standard deviation of 0.8. CanESM5 and MPI-ESM-1-2-HAM had negative correlations of -0.08 and -0.04, respectively. ACCESS-ESM1-5 and UKESM1-0-LL had correlation coefficients of 0.04 and 0.27, RMSDs of 2.3 and 2.6, and standard deviations of 2.1 and 2.7, respectively.

The performance of the ESMs in simulating nitrate concentrations was moderate to poor **(Fig. 6c)**. MPI-ESM1-2-HR, MPI-ESM1-2-LR, and MPI-ESM-1-2-HAM were the best performing models, with correlation coefficients of 0.24, 0.35, and 0.39, RMSDs of 0.99, 0.95, and 0.95, and standard deviations of 0.5, 0.19, and 0.16, respectively. MIROC-ES2L, NorESM2-MM, and UKESM1-0-LL had negative correlations of -0.07, -0.02, and -0.15, respectively. ACCESS-ESM1-5 had a correlation coefficient of 0.42, an RMSD of 9.24, and a standard deviation of 9.49. It's worth noting that, due to the NSD range limit, ACCESS-ESM1-5 is not visible in the **Fig. 6c**. All ESMs simulated oxygen concentrations with positive correlations **(Fig. 6d)**. MPI-ESM1-2-LR and UKESM1-0-LL were the best performing models, with correlation coefficients of 0.57 and 0.52, RMSDs of 1.29 and 1.38, and standard deviations of 1.57 and 1.6, respectively. ACCESS-ESM1-5 had the poorest performance, with a correlation coefficient of 0.58, an RMSD of 2.33, and a standard deviation of 2.75.

Overall, the performance of the ESMs in simulating biogeochemical variables was moderate to poor **(Table 2)**. MIROC-ES2H and MIROC-ES2L were the best performing models for chlorophyll and phytoplankton, while MPI-ESM1-2-HR, MPI-ESM1-2-LR, and MPI-ESM-1-2-HAM were the best performing models for nitrate. ACCESS-ESM1-5 generally performed poorly across all variables.

https://doi.org/10.5194/egusphere-2024-72
Preprint. Discussion started: 28 February 2024

Table 2. Spatial statistics for the 13 CMIP6 ESMs and their Ensemble.

CMIP6 ESMs	chlorophyll			phytoplankton			nitrate			oxygen		
	CC	NSD	NRMSD	CC	NSD	NRMSD	CC	NSD	NRMSD	CC	NSD	NRMSD
Model Ensemble	0.34	1.03	1.16	0.24	1.06	1.27	0.42	3.03	2.76	0.53	1.86	1.58
ACCESS-ESM1-5	0.10	2.01	2.15	0.04	2.14	2.33	0.30	9.49	9.24	0.58	2.75	2.33
CanESM5	-0.11	0.54	1.19	-0.08	0.58	1.20	0.07	0.07	1.00	0.72	2.34	1.77
CanESM5-CanOE	0.40	2.01	1.85	0.37	2.39	2.23	0.20	1.08	1.32	0.71	2.35	1.78
GFDL-ESM4	0.43	1.56	1.45	0.43	1.74	1.59	0.64	3.89	3.34	0.61	1.90	1.52
MIROC-ES2H	0.62	0.65	0.78	0.46	0.82	0.96	0.45	1.38	1.29	0.50	2.23	1.94
MIROC-ES2L	0.40	0.60	0.93	0.22	0.76	1.12	-0.07	2.23	2.51	0.42	2.40	2.18
MPI-ESM1-2-HR	0.07	1.20	1.51	0.01	1.27	1.61	0.24	0.05	0.99	0.59	2.01	1.63
MPI-ESM1-2-LR	0.13	0.95	1.29	0.02	1.19	1.54	0.35	0.19	0.95	0.57	1.57	1.29
MPI-ESM-1-2-HAM	0.04	1.22	1.54	-0.04	1.48	1.82	0.39	0.16	0.95	0.59	1.80	1.45
MRI-ESM2-0	0.29	0.89	1.13	0.20	1.10	1.33	0.18	4.18	4.12	0.30	1.80	1.78
NorESM2-LM	0.15	0.73	1.15	0.22	0.93	1.21	0.07	2.91	3.01	0.58	2.34	1.93
NorESM2-MM	0.13	0.84	1.22	0.18	1.05	1.32	-0.02	3.37	3.53	0.54	1.95	1.65
UKESM1-0-LL	0.20	1.73	1.81	0.28	2.77	2.67	-0.15	2.81	3.12	0.52	1.60	1.38

https://doi.org/10.5194/egusphere-2024-72
Preprint. Discussion started: 28 February 2024

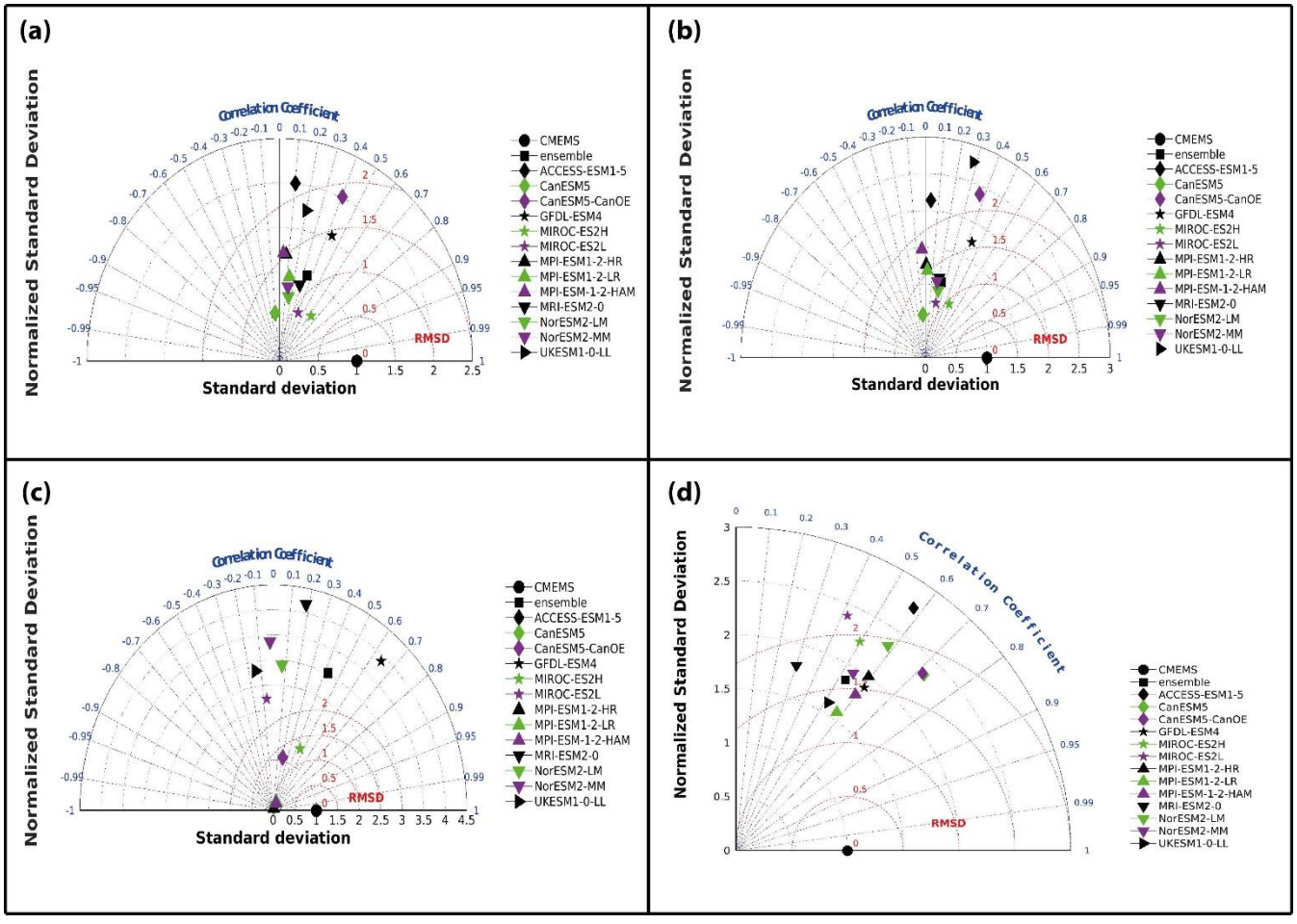

Figure 6. Annual Taylor Diagram for (a) chlorophyll, (b) phytoplankton, (c) nitrate and (d) oxygen.

4.3 Model ranking

In addition to the qualitative analysis presented in the Taylor diagram above, a skill score is calculated using Equation (5) to further validate the models' proficiency in reproducing biogeochemical variables. The Taylor skill score, derived from Equation (5), serves as a quantitative summary of the information conveyed by the Taylor diagram, providing a synthetic measure of the models' performance. The final ranking of models is determined based on this skill score. The ranking process involves assessing the skill score for each model with respect to individual variables. Subsequently, the average of the individual variable scores for each model is computed, serving as the overall score for that particular model. The final and variable scores for the models are depicted in the **Fig. 7**. A Taylor skill score closer to 1 indicates a higher agreement between the simulation and observation. This approach, akin to previous successful studies (Kim et al., 2023; Yool et al., 2021), enhances the robustness of the assessment.

https://doi.org/10.5194/egusphere-2024-72
Preprint. Discussion started: 28 February 2024

The overall performance of the selected CMIP6 ESMs is summarized in the final score graph **(Fig. 7a)**. MIROC-ES2H emerged as the top-ranked ESM, followed by GFDL-ESM4 and CanESM5-CanOE in second and third place, respectively. Beyond the top three, the final score curve exhibits a nearly linear pattern, suggesting that the remaining ESMs exhibited relatively consistent performance across various evaluation criteria. Notably, ACCESS-ESM1-5 ranked lowest among the ESMs, consistent with its observed performance in spatial bias and Taylor diagram analysis. MIROC-ES2H demonstrated superior performance across all variables except oxygen, consistently achieving scores above 0.2. For oxygen, MPI-ESM1-2-LR ranked highest due to its exceptional spatial representation and accurate seasonal pattern captured in the Taylor diagram. The distribution of scores for chlorophyll, phytoplankton, oxygen and nitrate **(Fig. 7b-e)** indicates that only a few ESMs consistently achieved top performance for these variables. Since an ensemble always masks the significant differences between the individual models, the Multi-Model Ensemble comprising of all ESMs does not take into account the relative strengths and weaknesses of each model (Bannister et al., 2017; Knutti, 2010). Therefore, evaluating GCMs in order to choose the best or most appropriate ones is crucial and helps planners and policymakers feel confident in their use of GCMs for impact assessment studies and other uses (Aloysius et al., 2016; Perez et al., 2014; Raju and Kumar, 2020).

https://doi.org/10.5194/egusphere-2024-72
Preprint. Discussion started: 28 February 2024

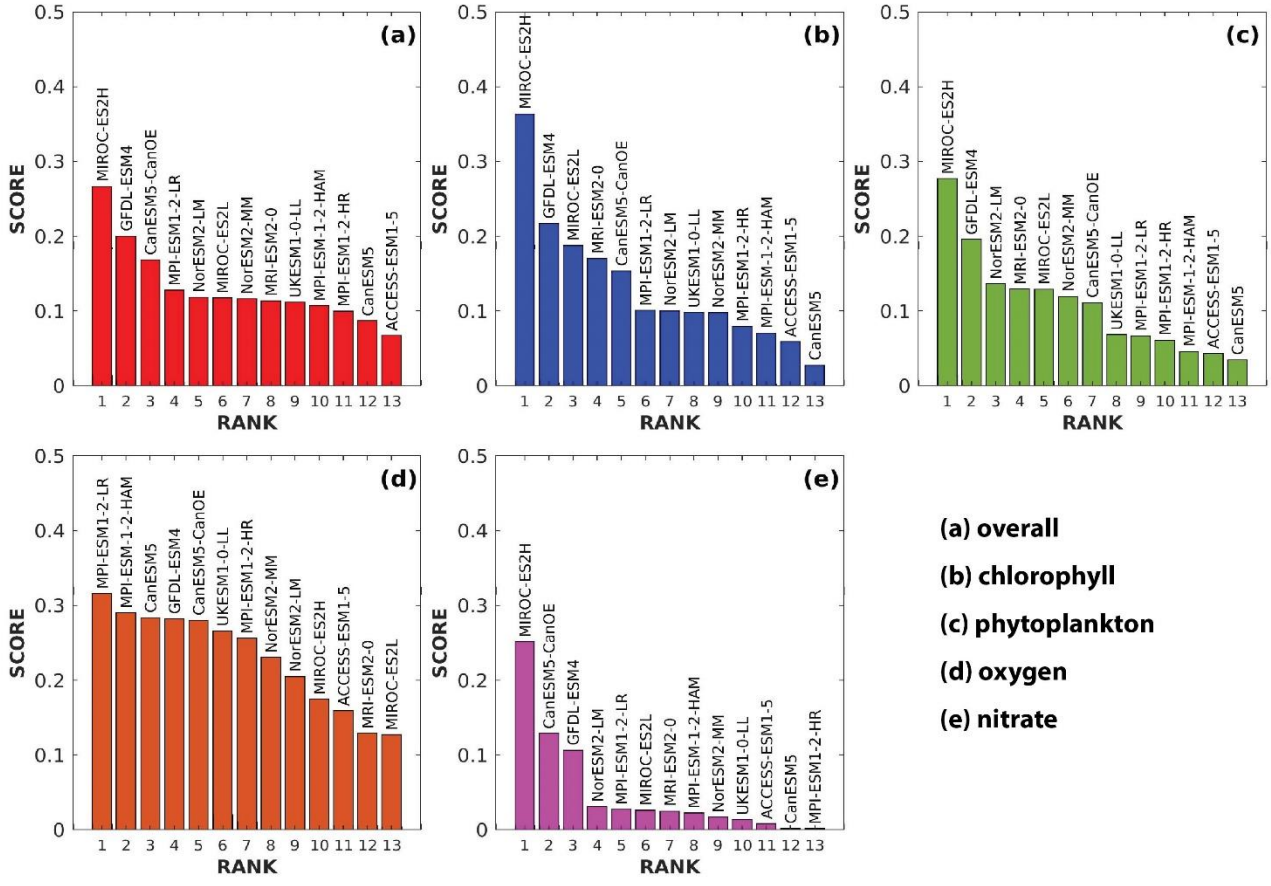

Figure 7. Selected CMIP6 ESMs' scores and ranks.

5 CONCLUSION

This study assessed the ability of 13 CMIP6 ESMs and their ensemble mean to replicate biogeochemical variables such as chlorophyll, phytoplankton, nitrate and oxygen over the southern SCS at annual and seasonal scales. The models and their ensemble mean were compared against CMEMS data, considered a proxy for observations for the period 1993-2014. Their performance was evaluated based on their ability to reproduce the seasonal climatology and distribution bias using statistical metrics such as the Taylor diagram and Taylor skill score. The models were ranked based on their skill score. The results revealed that some models slightly overestimated or underestimated biogeochemical variables during both seasons. The performance of the models varied between seasonal and annual scales. Most of the models exhibited a positive spatial correlation with CMEMS at both seasonal and annual scales. However, a few models showed negative correlations, such as CanESM5 (-0.11 and -0.08 for chlorophyll and phytoplankton, respectively), MPI-ESM-1-2-HAM (-0.04 for

https://doi.org/10.5194/egusphere-2024-72
Preprint. Discussion started: 28 February 2024

phytoplankton), MIROC-ES2L (-0.07 for nitrate), NorESM2-MM (-0.02 for nitrate), and UKESM1-0-LL (-0.15 for nitrate). Despite their overall good performance in the ranking, some models were unable to accurately simulate the seasonal climatology of the study region. While both Taylor diagram and Taylor skill score methods aim to assess model performance, discrepancies in model ranking can arise due to their different approaches. The Taylor diagram emphasizes a balanced assessment of correlation, RMSE, and SD, providing a visual representation of model performance and allowing for qualitative assessment and identification of strengths and weaknesses. In contrast, the Taylor skill score places more emphasis on RMSE and SD, as their normalized differences contribute more significantly to the numerical score, which may not capture the nuances of model performance observed in the Taylor diagram. Considering all these factors, the top five overall best-performing models for biogeochemical variables in southern SCS were MIROC-ES2H, GFDL-ESM4, CanESM5-CanOE, MPI-ESM1-2-LR, and NorESM2-LM. The conclusions drawn from this research hold significant implications for both researchers and policy-makers relying on the datasets. The outcomes offer valuable insights that can guide improvements in parameterization schemes within models, particularly in instances where the observed patterns were not effectively reproduced. Addressing the existing challenges related to topography and local-scale convective effects remains a priority for ongoing model enhancements.

DATA AVAILABILITY

The CMIP6 data are available from the Earth System Grid Federation (ESGF) https://esgf-node.llnl.gov/search/cmip6/. The reference CMEMS data can be accessed at https://data.marine.copernicus.eu/products.

AUTHOR CONTRIBUTIONS

The work, methodologies and formal analysis were conceptualized by W.M and J.X.C. The manuscript was authored by W.M, with input from all co-authors. Work supervision was conducted by M.F.A. All authors participated in contributing to the article and endorsed the submitted version.

CONFLICT OF INTEREST

The authors declare that the research was conducted in the absence of any commercial or financial relationships that could be construed as a potential conflict of interest.

FUNDING

This research was funded by Ministry of Higher Education (MoHE), Malaysia research grant under the Long Term Research Grant (LRGS) Scheme. Grant number: LRGS/1/2020/UMT/01/1/2.

https://doi.org/10.5194/egusphere-2024-72
Preprint. Discussion started: 28 February 2024

ACKNOWLEDGMENTS

The authors would like to acknowledge Long-Term Research Grant (LRGS), provided from Ministry of Higher Education (MoHE), Malaysia (LRGS/1/2020/UMT/01/1/2). We also acknowledge CMEMS (Copernicus Marine Environment Monitoring Service) for freely providing biogeochemical products and the World Climate Research Programme, which, through its Working Group on Coupled Modelling, coordinated and promoted CMIP6. We thank the climate modeling groups for producing and making available their model output, the Earth System Grid Federation (ESGF) for archiving the data and providing access, and the multiple funding agencies who support CMIP6 and ESGF.

REFERENCES

Aloysius, N. R., Sheffield, J., Saiers, J. E., Li, H., and Wood, E. F.: Evaluation of historical and future simulations of precipitation and temperature in central Africa from CMIP5 climate models, J. Geophys. Res., 121, https://doi.org/10.1002/2015JD023656, 2016.

Bannister, D., Herzog, M., Graf, H. F., Scott Hosking, J., and Short, C. A.: An assessment of recent and future temperature change over the Sichuan basin, China, using CMIP5 climate models, J. Clim., 30, https://doi.org/10.1175/JCLI-D-16-0536.1, 2017.

Chi, H., Wu, Y., Zheng, H., Zhang, B., Sun, Z., Yan, J., Ren, Y., and Guo, L.: Spatial patterns of climate change and associated climate hazards in Northwest China, Sci. Rep., 13, 10418, https://doi.org/10.1038/s41598-023-37349-w, 2023.

Christian, J. R., Denman, K. L., Hayashida, H., Holdsworth, A. M., Lee, W. G., Riche, O. G. J., Shao, A. E., Steiner, N., and Swart, N. C.: Ocean biogeochemistry in the Canadian Earth System Model version 5.0.3: CanESM5 and CanESM5-CanOE, Geosci. Model Dev., 15, 4393–4424, https://doi.org/10.5194/gmd-15-4393-2022, 2022.

Crameri, F., Shephard, G. E., and Heron, P. J.: The misuse of colour in science communication, Nat. Commun., 11, https://doi.org/10.1038/s41467-020-19160-7, 2020.

Crameri, F., Shephard, G., and Heron, P.: The “Scientific colour map” Initiative: Version 7 and its new additions, in: EGU General Assembly 2021, online, 19–30 Apr 2021, 2021.

Daryabor, F., Tangang, F., and Juneng, L.: Simulation of Southwest Monsoon Current Circulation and Temperature in the East Coast of Peninsular Malaysia, Sains Malaysiana, 389–398 pp., 2014.

Daryabor, F., Samah, A. A., and Ooi, S. H.: Dynamical structure of the sea off the east coast of Peninsular Malaysia, Ocean Dyn., 65, 93–106, https://doi.org/10.1007/s10236-014-0787-5, 2015.

Dunne, J. P., Horowitz, L. W., Adcroft, A. J., Ginoux, P., Held, I. M., John, J. G., Krasting, J. P., Malyshev, S., Naik, V., Paulot, F., Shevliakova, E., Stock, C. A., Zadeh, N., Balaji, V., Blanton, C., Dunne, K. A., Dupuis, C., Durachta, J., Dussin, R., Gauthier, P. P. G., Griffies, S. M., Guo, H., Hallberg, R. W., Harrison, M., He, J., Hurlin, W., McHugh, C., Menzel, R., Milly, P. C. D., Nikonov, S., Paynter, D. J., Ploshay, J., Radhakrishnan, A., Rand, K., Reichl, B. G., Robinson, T., Schwarzkopf, D. M., Sentman, L. T., Underwood, S., Vahlenkamp, H., Winton, M., Wittenberg, A. T., Wyman, B., Zeng, Y., and Zhao, M.: The GFDL Earth System Model Version 4.1 (GFDL-ESM 4.1): Overall Coupled Model Description and Simulation Characteristics, J. Adv. Model. Earth Syst., 12, https://doi.org/10.1029/2019MS002015, 2020.

Gan, J., Liu, Z., and Liang, L.: Numerical modeling of intrinsically and extrinsically forced seasonal circulation in the China Seas: A kinematic study, J. Geophys. Res. Ocean., 121, 4697–4715, https://doi.org/10.1002/2016JC011800, 2016.

Hajima, T., Watanabe, M., Yamamoto, A., Tatebe, H., Noguchi, M. A., Abe, M., Ohgaito, R., Ito, A., Yamazaki, D., Okajima, H., Ito, A., Takata, K., Ogochi, K., Watanabe, S., and Kawamiya, M.: Development of the MIROC-ES2L Earth system model and the evaluation of biogeochemical processes and feedbacks, Geosci. Model Dev., 13, https://doi.org/10.5194/gmd-13-2197-2020, 2020.

Henson, S., Cole, H., Beaulieu, C., and Yool, A.: The impact of global warming on seasonality of ocean primary production,

Biogeosciences, 10, 4357–4369, https://doi.org/10.5194/bg-10-4357-2013, 2013.

Jia, Q., Jia, H., Li, Y., and Yin, D.: Applicability of CMIP5 and CMIP6 Models in China: Reproducibility of Historical Simulation and Uncertainty of Future Projection, J. Clim., 36, 5809–5824, https://doi.org/10.1175/JCLI-D-22-0375.1, 2023.

Jiang, S., Müller, M., Jin, J., Wu, Y., Zhu, K., Zhang, G., Mujahid, A., Rixen, T., Muhamad, M. F., Sia, E. S. A., Jang, F. H. A., and Zhang, J.: Dissolved inorganic nitrogen in a tropical estuary in Malaysia: transport and transformation, Biogeosciences, 16, 2821–2836, https://doi.org/10.5194/bg-16-2821-2019, 2019.

Kawamiya, M., Hajima, T., Tachiiri, K., Watanabe, S., and Yokohata, T.: Two decades of Earth system modeling with an emphasis on Model for Interdisciplinary Research on Climate (MIROC), https://doi.org/10.1186/s40645-020-00369-5, 2020.

Kim, H. H., Laufkötter, C., Lovato, T., Doney, S. C., and Ducklow, H. W.: Projected 21st-century changes in marine heterotrophic bacteria under climate change, Front. Microbiol., 14, https://doi.org/10.3389/fmicb.2023.1049579, 2023.

Knutti, R.: The end of model democracy?, Clim. Change, 102, https://doi.org/10.1007/s10584-010-9800-2, 2010.

Kwiatkowski, L., Torres, O., Bopp, L., Aumont, O., Chamberlain, M., Christian, J. R., Dunne, J. P., Gehlen, M., Ilyina, T., John, J. G., Lenton, A., Li, H., Lovenduski, N. S., Orr, J. C., Palmieri, J., Santana-Falcón, Y., Schwinger, J., Séférian, R., Stock, C. A., Tagliabue, A., Takano, Y., Tjiputra, J., Toyama, K., Tsujino, H., Watanabe, M., Yamamoto, A., Yool, A., and Ziehn, T.: Twenty-first century ocean warming, acidification, deoxygenation, and upper-ocean nutrient and primary production decline from CMIP6 model projections, Biogeosciences, 17, 3439–3470, https://doi.org/10.5194/bg-17-3439-2020, 2020.

Lee, T., Fournier, S., Gordon, A. L., and Sprintall, J.: Maritime Continent water cycle regulates low-latitude chokepoint of global ocean circulation, Nat. Commun., 10, 2103, https://doi.org/10.1038/s41467-019-10109-z, 2019.

Liu, K.-K., Chao, S.-Y., Shaw, P.-T., Gong, G.-C., Chen, C.-C., and Tang, T. Y.: Monsoon-forced chlorophyll distribution and primary production in the South China Sea: observations and a numerical study, Deep Sea Res. Part I Oceanogr. Res. Pap., 49, 1387–1412, https://doi.org/10.1016/S0967-0637(02)00035-3, 2002.

Lønborg, C., Müller, M., Butler, E. C. V., Jiang, S., Ooi, S. K., Trinh, D. H., Wong, P. Y., Ali, S. M., Cui, C., Siong, W. B., Yando, E. S., Friess, D. A., Rosentreter, J. A., Eyre, B. D., and Martin, P.: Nutrient cycling in tropical and temperate coastal waters: Is latitude making a difference?, Estuar. Coast. Shelf Sci., 262, 107571, https://doi.org/10.1016/j.ecss.2021.107571, 2021.

Lu, Z., Gan, J., Dai, M., Zhao, X., and Hui, C. R.: Nutrient transport and dynamics in the South China Sea: A modeling study, Prog. Oceanogr., 183, 102308, https://doi.org/10.1016/j.pocean.2020.102308, 2020.

Mauritsen, T., Bader, J., Becker, T., Behrens, J., Bittner, M., Brokopf, R., Brovkin, V., Claussen, M., Crueger, T., Esch, M., Fast, I., Fiedler, S., Fläschner, D., Gayler, V., Giorgetta, M., Goll, D. S., Haak, H., Hagemann, S., Hedemann, C., Hohenegger, C., Ilyina, T., Jahns, T., Jimenéz-de-la-Cuesta, D., Jungclaus, J., Kleinen, T., Kloster, S., Kracher, D., Kinne, S., Kleberg, D., Lasslop, G., Kornblueh, L., Marotzke, J., Matei, D., Meraner, K., Mikolajewicz, U., Modali, K., Möbis, B., Müller, W. A., Nabel, J. E. M. S., Nam, C. C. W., Notz, D., Nyawira, S. S., Paulsen, H., Peters, K., Pincus, R., Pohlmann, H., Pongratz, J., Popp, M., Raddatz, T. J., Rast, S., Redler, R., Reick, C. H., Rohrschneider, T., Schemann, V., Schmidt, H., Schnur, R., Schulzweida, U., Six, K. D., Stein, L., Stemmler, I., Stevens, B., von Storch, J. S., Tian, F., Voigt, A., Vrese, P., Wieners, K. H., Wilkenskjeld, S., Winkler, A., and Roeckner, E.: Developments in the MPI-M Earth System Model version 1.2 (MPI-ESM1.2) and Its Response to Increasing CO2, J. Adv. Model. Earth Syst., 11, https://doi.org/10.1029/2018MS001400, 2019.

Milliman, J. D., Farnsworth, K. L., and Albertin, C. S.: Flux and fate of fluvial sediments leaving large islands in the East Indies, J. Sea Res., 41, 97–107, https://doi.org/10.1016/S1385-1101(98)00040-9, 1999.

Mohanty, S., Bhattacharya, B., and Singh, C.: Spatio-temporal variability of surface chlorophyll and pCO2 over the tropical Indian Ocean and its long-term trend using CMIP6 models, Sci. Total Environ., 908, 168285, https://doi.org/10.1016/j.scitotenv.2023.168285, 2024.

Müller, W. A., Jungclaus, J. H., Mauritsen, T., Baehr, J., Bittner, M., Budich, R., Bunzel, F., Esch, M., Ghosh, R., Haak, H., Ilyina, T., Kleine, T., Kornblueh, L., Li, H., Modali, K., Notz, D., Pohlmann, H., Roeckner, E., Stemmler, I., Tian, F., and Marotzke, J.: A Higher-resolution Version of the Max Planck Institute Earth System Model (MPI-ESM1.2-HR), J. Adv. Model. Earth Syst., 10, https://doi.org/10.1029/2017MS001217, 2018.

Neubauer, D., Ferrachat, S., Siegenthaler-Le Drian, C., Stier, P., Partridge, D. G., Tegen, I., Bey, I., Stanelle, T., Kokkola,

https://doi.org/10.5194/egusphere-2024-72
Preprint. Discussion started: 28 February 2024

H., and Lohmann, U.: The global aerosol-climate model ECHAM6.3-HAM2.3-Part 2: Cloud evaluation, aerosol radiative forcing, and climate sensitivity, Geosci. Model Dev., 12, https://doi.org/10.5194/gmd-12-3609-2019, 2019.

Oh, S.-G., Kim, B.-G., Cho, Y.-K., and Son, S.-W.: Quantification of The Performance of CMIP6 Models for Dynamic Downscaling in The North Pacific and Northwest Pacific Oceans, Asia-Pacific J. Atmos. Sci., https://doi.org/10.1007/s13143-023-00320-w, 2023.

Palacz, A. P., Xue, H., Armbrecht, C., Zhang, C., and Chai, F.: Seasonal and inter-annual changes in the surface chlorophyll of the South China Sea, J. Geophys. Res., 116, C09015, https://doi.org/10.1029/2011JC007064, 2011.

Peng, W., Chen, Q., Zhou, S., and Huang, P.: CMIP6 model-based analog forecasting for the seasonal prediction of sea surface temperature in the offshore area of China, Geosci. Lett., 8, 8, https://doi.org/10.1186/s40562-021-00179-7, 2021.

Pereira, H., Picado, A., Sousa, M. C., Alvarez, I., and Dias, J. M.: Evaluation of Earth System Models outputs over the continental Portuguese coast: A historical comparison between CMIP5 and CMIP6, Ocean Model., 184, 102207, https://doi.org/10.1016/j.ocemod.2023.102207, 2023.

Perez, J., Menendez, M., Mendez, F. J., and Losada, I. J.: Evaluating the performance of CMIP3 and CMIP5 global climate models over the north-east Atlantic region, Clim. Dyn., 43, https://doi.org/10.1007/s00382-014-2078-8, 2014.

Perruche, C. ., Szczypta, C. ., Paul, J. ., and Drévillon, M. .: Quality Information Document (QuID) - Global Production Centre GLOBAL_REANALYSIS_BIO_001_029., Copernicus Mar. Environ. Monit. Serv., 2019.

Petrik, C. M., Luo, J. Y., Heneghan, R. F., Everett, J. D., Harrison, C. S., and Richardson, A. J.: Assessment and Constraint of Mesozooplankton in CMIP6 Earth System Models, Global Biogeochem. Cycles, 36, https://doi.org/10.1029/2022GB007367, 2022.

Raju, K. S. and Kumar, D. N.: Review of approaches for selection and ensembling of GCMS, https://doi.org/10.2166/wcc.2020.128, 2020.

Riahi, K., van Vuuren, D. P., Kriegler, E., Edmonds, J., O'Neill, B. C., Fujimori, S., Bauer, N., Calvin, K., Dellink, R., Fricko, O., Lutz, W., Popp, A., Cuaresma, J. C., KC, S., Leimbach, M., Jiang, L., Kram, T., Rao, S., Emmerling, J., Ebi, K., Hasegawa, T., Havlik, P., Humpenöder, F., Da Silva, L. A., Smith, S., Stehfest, E., Bosetti, V., Eom, J., Gernaat, D., Masui, T., Rogelj, J., Strefler, J., Drouet, L., Krey, V., Luderer, G., Harmsen, M., Takahashi, K., Baumstark, L., Doelman, J. C., Kainuma, M., Klimont, Z., Marangoni, G., Lotze-Campen, H., Obersteiner, M., Tabeau, A., and Tavoni, M.: The Shared Socioeconomic Pathways and their energy, land use, and greenhouse gas emissions implications: An overview, Glob. Environ. Chang., 42, 153–168, https://doi.org/10.1016/j.gloenvcha.2016.05.009, 2017.

von Schuckmann, K., Le Traon, P.-Y., Smith, N., Pascual, A., Djavidnia, S., Gattuso, J.-P., Grégoire, M., Nolan, G., Aaboe, S., Fanjul, E. Á., Aouf, L., Aznar, R., Badewien, T. H., Behrens, A., Berta, M., Bertino, L., Blackford, J., Bolzon, G., Borile, F., Bretagnon, M., Brewin, R. J. W., Canu, D., Cessi, P., Ciavatta, S., Chapron, B., Trang Chau, T. T., Chevallier, F., Chtirkova, B., Ciliberti, S., Clark, J. R., Clementi, E., Combot, C., Comerma, E., Conchon, A., Coppini, G., Corgnati, L., Cossarini, G., Cravatte, S., de Alfonso, M., de Boyer Montégut, C., De Lera Fernández, C., de los Santos, F. J., Denvil-Sommer, A., de Pascual Collar, Á., Dias Nunes, P. A. L., Di Biagio, V., Drudi, M., Embury, O., Falco, P., d'Andon, O. F., Ferrer, L., Ford, D., Freund, H., León, M. G., Sotillo, M. G., García-Valdecasas, J. M., Garnesson, P., Garric, G., Gasparin, F., Gehlen, M., Genua-Olmedo, A., Geyer, G., Ghermandi, A., Good, S. A., Gourrion, J., Greiner, E., Griffa, A., González, M., Griffa, A., Hernández-Carrasco, I., Isoard, S., Kennedy, J. J., Kay, S., Korosov, A., Laanemäe, K., Land, P. E., Lavergne, T., Lazzari, P., Legeais, J.-F., Lemieux, B., Levier, B., Llovel, W., Lyubartsev, V., Le Traon, P.-Y., Lien, V. S., Lima, L., Lorente, P., Mader, J., Magaldi, M. G., Maljutenko, I., Mangin, A., Mantovani, C., Marinova, V., Masina, S., Mauri, E., Meyerjürgens, J., Mignot, A., McEwan, R., Mejia, C., et al.: Copernicus Marine Service Ocean State Report, Issue 4, J. Oper. Oceanogr., 13, S1–S172, https://doi.org/10.1080/1755876X.2020.1785097, 2020.

Sellar, A. A., Jones, C. G., Mulcahy, J. P., Tang, Y., Yool, A., Wiltshire, A., O'Connor, F. M., Stringer, M., Hill, R., Palmieri, J., Woodward, S., de Mora, L., Kuhlbrodt, T., Rumbold, S. T., Kelley, D. I., Ellis, R., Johnson, C. E., Walton, J., Abraham, N. L., Andrews, M. B., Andrews, T., Archibald, A. T., Berthou, S., Burke, E., Blockley, E., Carslaw, K., Dalvi, M., Edwards, J., Folberth, G. A., Gedney, N., Griffiths, P. T., Harper, A. B., Hendry, M. A., Hewitt, A. J., Johnson, B., Jones, A., Jones, C. D., Keeble, J., Liddicoat, S., Morgenstern, O., Parker, R. J., Predoi, V., Robertson, E., Siahaan, A., Smith, R. S., Swaminathan, R., Woodhouse, M. T., Zeng, G., and Zerroukat, M.: UKESM1: Description

https://doi.org/10.5194/egusphere-2024-72
Preprint. Discussion started: 28 February 2024

and Evaluation of the U.K. Earth System Model, J. Adv. Model. Earth Syst., 11, https://doi.org/10.1029/2019MS001739, 2019.

Shikha, S. and Valsala, V.: Subsurface ocean biases in climate models and its implications in the simulated interannual variability: A case study for Indian Ocean, Dyn. Atmos. Ocean., 84, 55–74, https://doi.org/10.1016/j.dynatmoce.2018.10.001, 2018.

Sun, G. and Mu, M.: Impacts of two types of errors on the predictability of terrestrial carbon cycle, Ecosphere, 12, https://doi.org/10.1002/ecs2.3315, 2021.

Swart, N. C., Cole, J. N. S., Kharin, V. V., Lazare, M., Scinocca, J. F., Gillett, N. P., Anstey, J., Arora, V., Christian, J. R., Hanna, S., Jiao, Y., Lee, W. G., Majaess, F., Saenko, O. A., Seiler, C., Seinen, C., Shao, A., Sigmond, M., Solheim, L., Von Salzen, K., Yang, D., and Winter, B.: The Canadian Earth System Model version 5 (CanESM5.0.3), Geosci. Model Dev., 12, 4823–4873, https://doi.org/10.5194/gmd-12-4823-2019, 2019.

Tang, T., Luo, J.-J., Peng, K., Qi, L., and Tang, S.: Over-projected Pacific warming and extreme El Niño frequency due to CMIP5 common biases, Natl. Sci. Rev., 8, https://doi.org/10.1093/nsr/nwab056, 2021.

Taylor, K. E.: Summarizing multiple aspects of model performance in a single diagram, J. Geophys. Res. Atmos., 106, 7183–7192, https://doi.org/10.1029/2000JD900719, 2001.

Tjiputra, J. F., Schwinger, J., Bentsen, M., L. Morée, A., Gao, S., Bethke, I., Heinze, C., Goris, N., Gupta, A., He, Y. C., Olivié, D., Seland, O., and Schulz, M.: Ocean biogeochemistry in the Norwegian Earth System Model version 2 (NorESM2), Geosci. Model Dev., 13, https://doi.org/10.5194/gmd-13-2393-2020, 2020.

Todd, P. A., Heery, E. C., Loke, L. H. L., Thurstan, R. H., Kotze, D. J., and Swan, C.: Towards an urban marine ecology: characterizing the drivers, patterns and processes of marine ecosystems in coastal cities, Oikos, 128, 1215–1242, https://doi.org/10.1111/oik.05946, 2019.

Tseng, C., Wong, G. T. F., Lin, I. -I., Wu, C. -R., and Liu, K. -K.: A unique seasonal pattern in phytoplankton biomass in low-latitude waters in the South China Sea, Geophys. Res. Lett., 32, https://doi.org/10.1029/2004GL022111, 2005.

Yool, A., Palmiéri, J., Jones, C. G., de Mora, L., Kuhlbrodt, T., Popova, E. E., Nurser, A. J. G., Hirschi, J., Blaker, A. T., Coward, A. C., Blockley, E. W., and Sellar, A. A.: Evaluating the physical and biogeochemical state of the global ocean component of UKESM1 in CMIP6 historical simulations, Geosci. Model Dev., 14, 3437–3472, https://doi.org/10.5194/gmd-14-3437-2021, 2021.

You, Y. and Ting, M.: Low Pressure Systems and Extreme Precipitation in Southeast and East Asian Monsoon Regions, J. Clim., 34, 1147–1162, https://doi.org/10.1175/JCLI-D-20-0206.1, 2021.

Yukimoto, S., Kawai, H., Koshiro, T., Oshima, N., Yoshida, K., Urakawa, S., Tsujino, H., Deushi, M., Tanaka, T., Hosaka, M., Yabu, S., Yoshimura, H., Shindo, E., Mizuta, R., Obata, A., Adachi, Y., and Ishii, M.: The meteorological research institute Earth system model version 2.0, MRI-ESM2.0: Description and basic evaluation of the physical component, J. Meteorol. Soc. Japan, 97, https://doi.org/10.2151/jmsj.2019-051, 2019.

Ziehn, T., Chamberlain, M. A., Law, R. M., Lenton, A., Bodman, R. W., Dix, M., Stevens, L., Wang, Y.-P., and Srbinovsky, J.: The Australian Earth System Model: ACCESS-ESM1.5, J. South. Hemisph. Earth Syst. Sci., 70, 193–214, https://doi.org/10.1071/ES19035, 2020.